X-922-77-260
PREPRINT

TM-78039

A METHOD OF INVERSION OF SATELLITE MAGNETIC ANOMALY DATA

M. A. MAYHEW

OCTOBER 1977

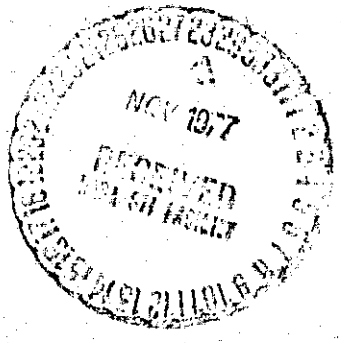

GSFC — GODDARD SPACE FLIGHT CENTER —
GREENBELT, MARYLAND

X-922-77-260

A METHOD OF INVERSION OF SATELLITE MAGNETIC ANOMALY DATE

M.A. Mayhew

Geophysics Branch
NASA Goddard Space Flight Center
Greenbelt, Maryland 20771

Based on Presentation at IAGA Meeting
Seattle, WA. - August 1976
To be published in the Journal of Geophysics

ABSTRACT

A method of finding a first approximation to a crustal magnetization distribution from inversion of satellite magnetic anomaly data is described. Magnetization is expressed as a Fourier Series in a segment of spherical shell. Input to this procedure is an equivalent source representation of the observed anomaly field. Instability of the inversion occurs when high frequency noise is present in the input data, or when the series is carried to an excessively high wave number. Preliminary results are given for the United States and adjacent areas.

INTRODUCTION

The polar-orbiting satellites OGO 2, 4, and 6 collected total-field magnetic data at elevations above 400km. A preliminary anomaly data set was created by selecting data with minimal external field effects, and by subtracting a 13^{th} degree spherical harmonic representation of the core field fit to this data subset. Regan et al (1975) published a 1^{o}-average representation of the anomaly field for a strip around the world between 50^{o}N and 50^{o}S, and described the data reduction procedures.

This paper is a review of a simple method for finding a first approximation to a crustal magnetization distribution which will produce a field which reproduces the measured satellite field. The term "crust" is used loosely to mean a layer bounded by the Earth's surface and the Curie isotherm, and may or may not correspond to the petrologic crust in a given area.

MODELING THE ANOMALY FIELD

The anomaly data set is contaminated by noise of three main kinds: 1) instrument noise, 2) local current effects, and 3) very long wavelength effects due to magnetospheric ring currents. The third effect has been described by Langel and Sweeney (1971). Cain and Davis (1973) modeled this effect as a first zonal harmonic, which they fit to individual satellite passes between 50^{o}N and 50^{o}S geomagnetic. Figure 1 is three groups of three passes in profile form; the tracks are shown i Figure 2. Within each group the satellite elevations are similar, and t the profiles should be similar. The raw anomaly data is shown in row 1 clearly, residual long wavelength effects are present in the individua profiles. Row 2 is "ring-corrected" data. The correction generally

improves the internal agreement, but a substantial residual remains, and some further correction is needed. This residual is partly responsible for the north-south elongation of anomaly contours, reflecting the satellite tracks, in the world map of Regan et al (1975). The result is effective high frequency noise in the east-west direction. In rows 3 and 4 linear and quadratic functions, respectively, have been fit to the individual profiles and subtracted. In row 5, a first zonal harmonic term has been fit only over the latitude range shown. The internal agreement is greatly improved in each case, but seems slightly better for the quadratic fit; therefore, a quadratic function was fit to and subtracted from each profile used in the computations described below.

The data is distributed through a considerable elevation range, but we would like to be able to represent the field at an arbitrary constant elevation. For this reason, and to average out instrumental and transient current effects, the anomaly field was modeled by an equivalent source procedure. This consisted of setting out an array of dipoles at the Earth's surface in a 4^{0} latitude-longitude grid, and determining a set of moments for the dipoles which would generate an artificial field which would make a least-squares best fit to the data; the mathematics is outlined in the Appendix. The dipoles were oriented along the direction of the main field, although to simply model the field this direction is not critical. The input data was limited to the elevation range 400-550 km. The fit of the computed field to the data is to a standard deviation of about 1 nT. Once the dipole moments are determined, the field can be computed at any elevation; a computation

at 450 km is shown in Figure 3. Figure 4 shows the fit of observed and computed fields for an arbitrary selection of profiles running between 10^{o}N and 50^{o}N in the area of Figure 3.

The input field to the inversion procedure outlined below must be smooth. Since the equivalent source field fills this requirement, it, rather than the raw anomaly data, was so used.

MAGNETIZATION DISTRIBUTION

The set of magnetic moments determined in the equivalent source computation vary irregularly, and have no particular physical significance. One approach to developing a physically meaningful model of the magnetic source distribution is to seek a continuous distribution of magnetization in a layer of constant thickness which will give rise to a field which closely fits the input field. The result is a first approximation to gross magnetization variations in the magnetic crust. The procedure is similar to that for the equivalent source computations described above, but with two essential differences. First, the sources are 2^{o} blocks 40 km thick, rather than dipoles. An approximate source function was developed for the anomaly due to such spherical prisms (see Appendix). Second, rather than allowing the moments of the sources to vary independently, their magnetizations were specified by the value of a double Fourier series in latitude and longitude having terms of the form

$$A_{ij} \cdot (\cos,\sin)(2\pi ix/X) \cdot (\cos,\sin)(2\pi jy/Y). \qquad (1)$$

The unknown parameters in the least-squares formulation are then the

constants of the series, rather than the magnetic moments of individual sources. Map areas 40^{o} by 40^{o} were treated individually. The equivalent source field, tapered to zero 4^{o} beyond each map border, was used for input. The Fourier series was expressed within the extended area; thus, in expression (1) above $X=Y=48^{o}$.

Once the series parameters are determined, the field can be computed at arbitrary elevation. The result at 450 km is shown in Figure 5, which is to be compared with Figure 3. The magnetization distribution itself in units of emu/cc x 10^{4} is shown in Figure 6.

There is a particular advantage to having the data so high above the sources. A particular source block has very nearly the same anomaly as a block twice the thickness and half the magnetization; thus, one can readily convert the model of magnetization variation in a layer of constant thickness to variations in a layer of variable thickness where there is independent evidence on the thickness of the magnetic crust.

SOURCES OF INSTABILITY

High frequency components of the field tend to be strongly amplified on inversion. Two examples of difficulties of this type are discussed below.

The map on the left in Figure 7, a test area in the Indian Ocean, was made by averaging corrected data within the elevation range 400-550 km over 1^{o} squares; average data generally contains high frequency noise contamination. The southern part of the map is in high magnetic latitudes, and external field noise is present along the southern border. The map on the right is the result of an inversion in which

these components have evidently been exaggerated, producing a characteristic cell-like structure.

Figure 8 shows a second kind of problem. There is an obvious question of how large the maximum wave number in the Fourier representation of magnetization can be. Figure 8 shows the results of computations for maximum wave number 3,4,5 and 6. The maps in the top row are the magnetization results; shown below are the corresponding power spectra. Note that while the low frequency part of the spectrum does not change very much, for m=5 and 6 increasing energy is entering the high frequency part. Apparently spurious effects appear in the corresponding magnetization maps. It would seem, then, that for an area this size the maximum appropriate wave number is 4, despite the fact that the fit of input to computed values continues to improve with expanding series, as indicated by the standard deviation values. The result suggests the limits of source resolution with this method. m=4 corresponds to a minimum wavelength of roughly twice the elevation of the data. The results of Figure 6 were computed for m=5, which corresponds to about the same minimum wavelength because the map area is larger.

ACKNOWLEDGMENTS

This work was done as part of the NASA-U.S. Geological Survey program for interpretation of satellite magnetic data. W.M. Davis of USGS has been largely responsible for preparation of the data set used in this study. The author was supported by a Research Associateship from the National Academy of Sciences.

REFERENCES

Cain, J.C., Hendricks, S.J., Langel, R.A., and Hudson, W.V., 1967, A Proposed Model for the International Geomagnetic Reference Field - 1965: J. Geomag. and Geoelect., v. 19, pp. 335-355.

Cain, J.C., and Davis, W.M., 1973, Low Latitude Variations of the Magnetic Field: in Symposium on Low Level Satellite Surveys, Internat'l. Assoc. of Geomagnetism and Aeronomy, Paris, pp. 67-87.

Eaton, G.P., Prostka, H.J., Oriel, S.S., and Pierce, K.L., 1976, Cordilleran Thermotectonic Anomaly: I. Geophysical and Geological Evidence of Coherent Late Cenozoic Intraplate Magmatism and Deformation: Geol. Soc. America Abstr. with Programs, v. 8, p. 850.

Ervin, C.P., and McGinnis, L.D., 1975, Reelfoot Rift: Reactivated Precursor to the Mississippi Embayment: Bull. Geol. Soc. Amer., v. 86, pp. 1287-1295.

Gradshteyn, I.S., and Ryzhik, I.M., 1965. Table of Integrals, Series and Products (A. Jeffrey,ed.): Academic Press, p. 83.

Langel R.A., and Sweeney, R.E., 1971, Asymmetric Ring Current at Twilight Local Time: J. Geoph. Res., v. 76, pp. 4420-4427.

Regan, R.D., Cain, J.C., and Davis, W.M., 1975, A Global Magnetic Anomaly Map: J. Geoph. Res., v. 80, pp. 794-802.

APPENDIX

Equivalent Source Field

We seek an expression for the potential of a dipole located at a point j on the Earth's surface at some external measurement point i. Specify the coordinates as (r_j, θ_j, ϕ_j) and (r_i, θ_i, ϕ_i), where r is radial distance, θ is colatitude, and ϕ is longitude east.

$$V_{ij} = -\bar{m}_j \cdot \nabla \frac{1}{\ell_{ij}} \quad ,$$

where ℓ_{ij} is the distance between i and j.

$$\ell_{ij}^2 = r_j^2 + r_i^2 - 2r_j r_i \cos\zeta_{ij} \quad ,$$

where ζ_{ij} is the central angle between i and j, and

$$\cos\zeta_{ij} = \cos\theta_j \cos\theta_i + \sin\theta_j \sin\theta_i \cos(\phi_i - \phi_j).$$

The components of $\bar{m}_j$ are

$$(m_j \sin I,\ m_j \cos I \cos D,\ m_j \cos I \sin D),$$

where I and D are inclination and declination of the dipole, taken to be that of the main field vector at the dipole.

Differentiation and substitution yields

$$V_{ij} = m_j(\sin I(r_j - r_i A) + \cos I \cos D r_i B - \cos I \sin D r_i C)/\ell_{ij}^3 \quad ,$$

where $A = \cos\theta_j \cos\theta_i + \sin\theta_j \sin\theta_i \cos(\phi_i - \phi_j)$

$B = \sin\theta_j \cos\theta_i - \cos\theta_j \sin\theta_i \cos(\phi_i - \phi_j)$

$C = \sin\theta_i \sin(\phi_i - \phi_j).$

The gradient of V_{ij} in the total field direction is the anomaly in the total field, B_{ij}.

The anomaly due to all the dipoles is

$$F_i = \sum_j m_j B_{ij} \ .$$

Using a procedure outlined by Cain et al (1967), we determine a set of values for the m_j which will minimize the square residuals between observed and measured F over all points i.

Field due to Spherical Prison of Elemental Area

Proceeding from the dipole result, we write down an expression for the potential of a volume element.

$$dV_{ij} = \frac{1}{\ell_{ij}^3} \left(J_r(r_j - r_i A) + J_\theta r_i B - J_\phi r_i C \right) r_j^2 \sin\theta_j \, d\theta_j \, d\phi_j \, dr_j \ ,$$

where (J_r, J_θ, J_ϕ) is the magnetization vector.
Then integrating in the r direction, and replacing the infinitesimal angles by small finite angles gives the potential of a spherical prism of elemental area,

$$\Delta V_{ij} = J_r \sin\theta_j \Delta\theta_j \Delta\phi_j \int_{R_1}^{R_2} \frac{r_j^3}{\ell_{ij}^3} \, dr_j$$

$$+ (-J_R r_i A + J_\theta r_i B - J_\phi r_i C) \sin\theta_j \Delta\theta_j \Delta\phi_j \int_{R_1}^{R_2} \frac{r_j^2}{\ell_{ij}^3} \, dr_j \ ,$$

where $(R_2 - R_1) = 40$ km, the approximate "crustal" thickness used in this paper. Experiments with computations have shown that the $\Delta\theta$ and $\Delta\phi$ can be taken to be 2^o in the above expression, and still give an excellant approximation to the field of a prism with finite angular dimensions.

The integrals above are given by Gradshteyn and Ryzhik (1965); the expressions are fairly lengthy, and are not reproduced here.

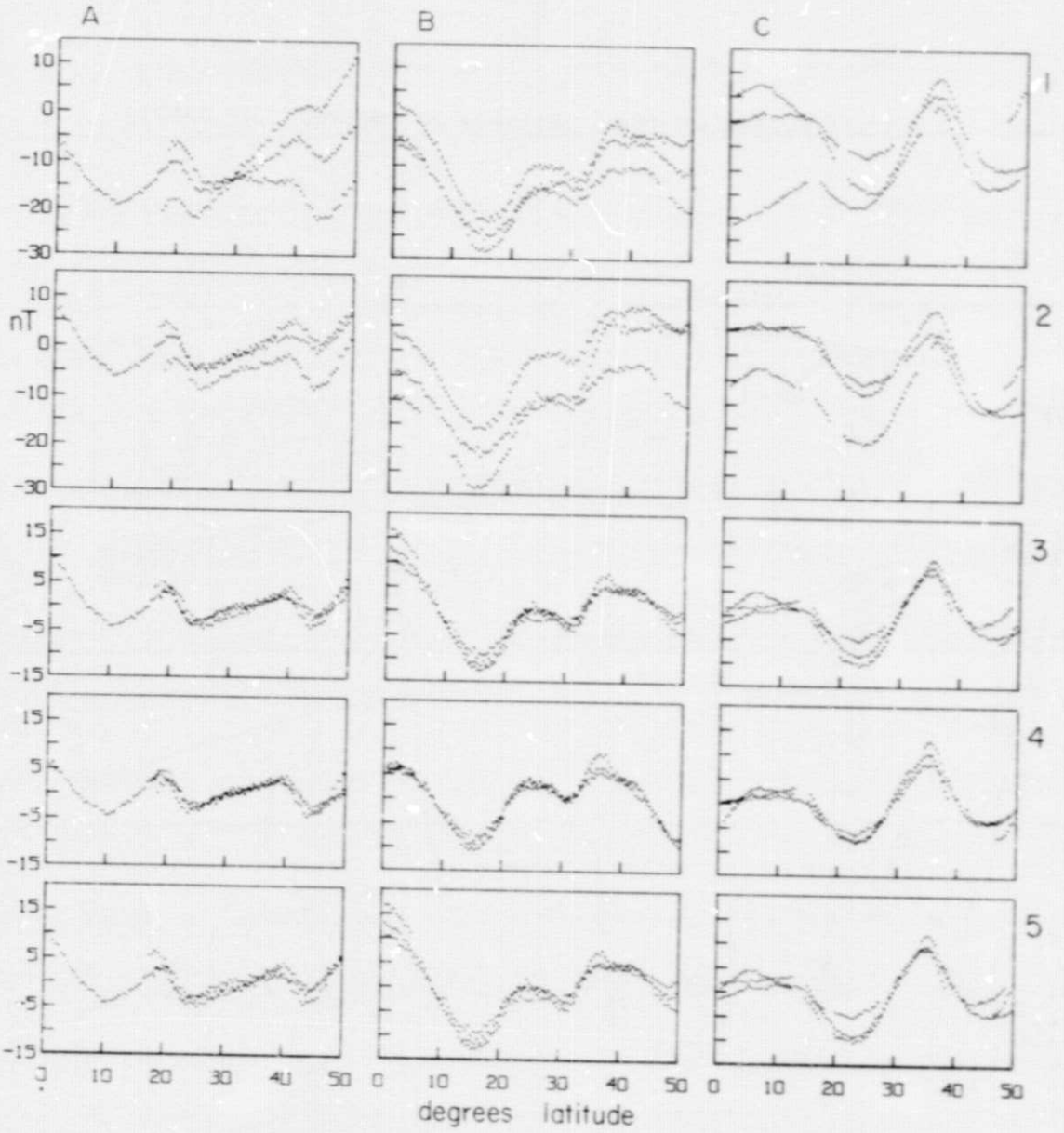

Figure 1: Satellite magnetic anomaly profiles; locations shown in Figure 2. Row 1, raw anomaly data. Rows 2-5, anomalies with corrections described in text.

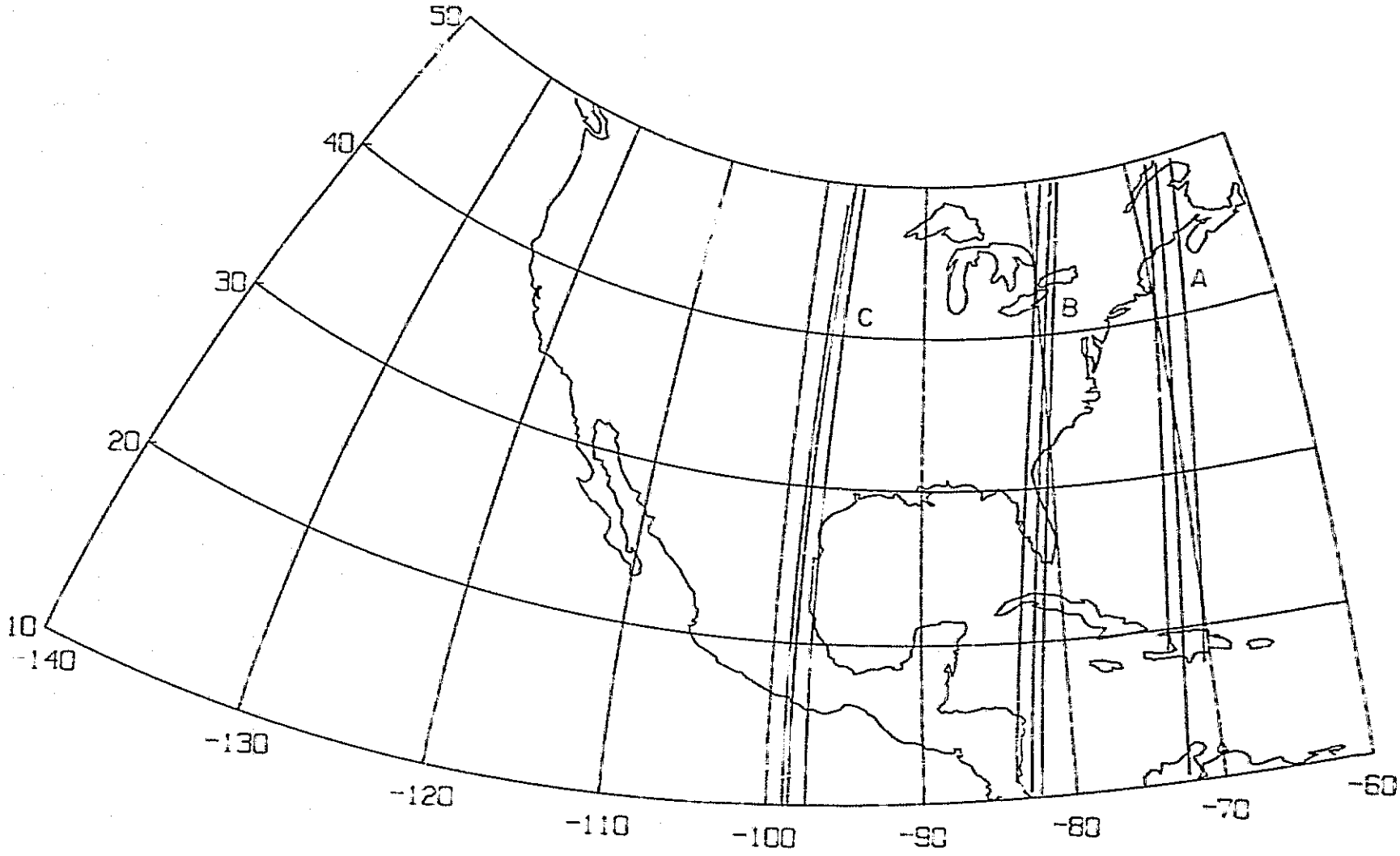

Figure 2: Location of Profiles shown in Figure 1.

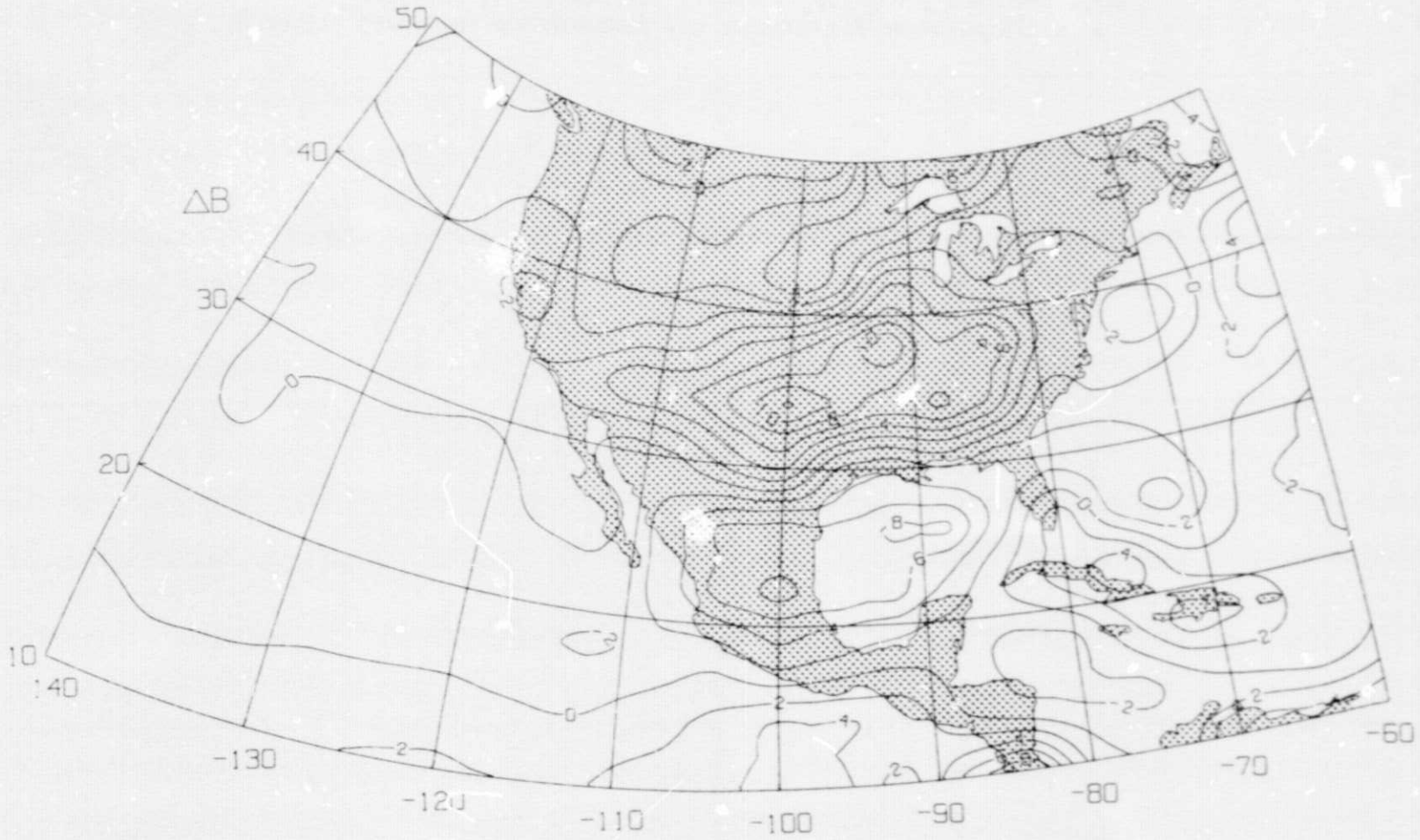

Figure 3: Equivalent source anomaly field computed at 450 km elevation
Units are nT.

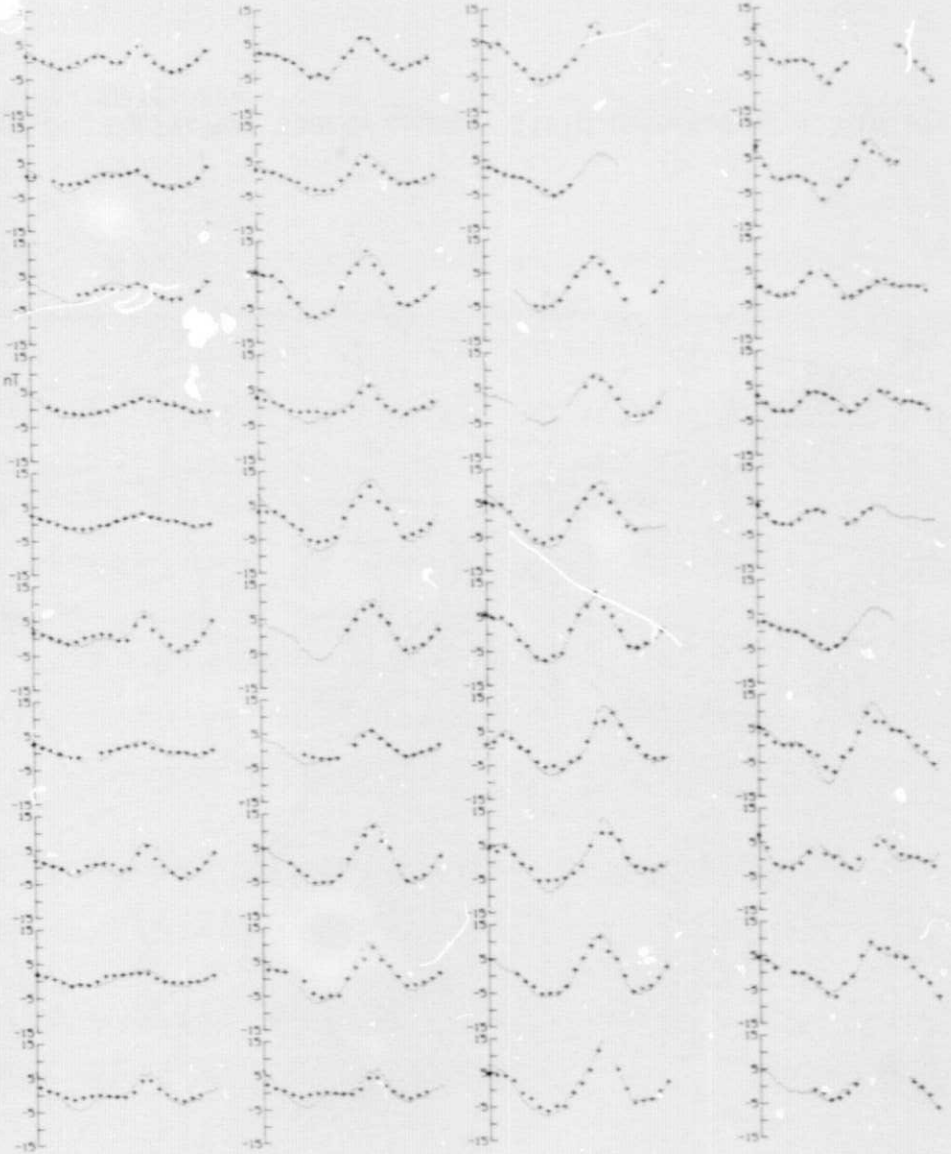

Figure 4: Corrected measurements for arbitrarily selected group of profiles in the area of Figure 3 (dots) and computed values (pluses). Computations cease where profile passes out of geographic area or (more commonly) rises above 550 km elevation.

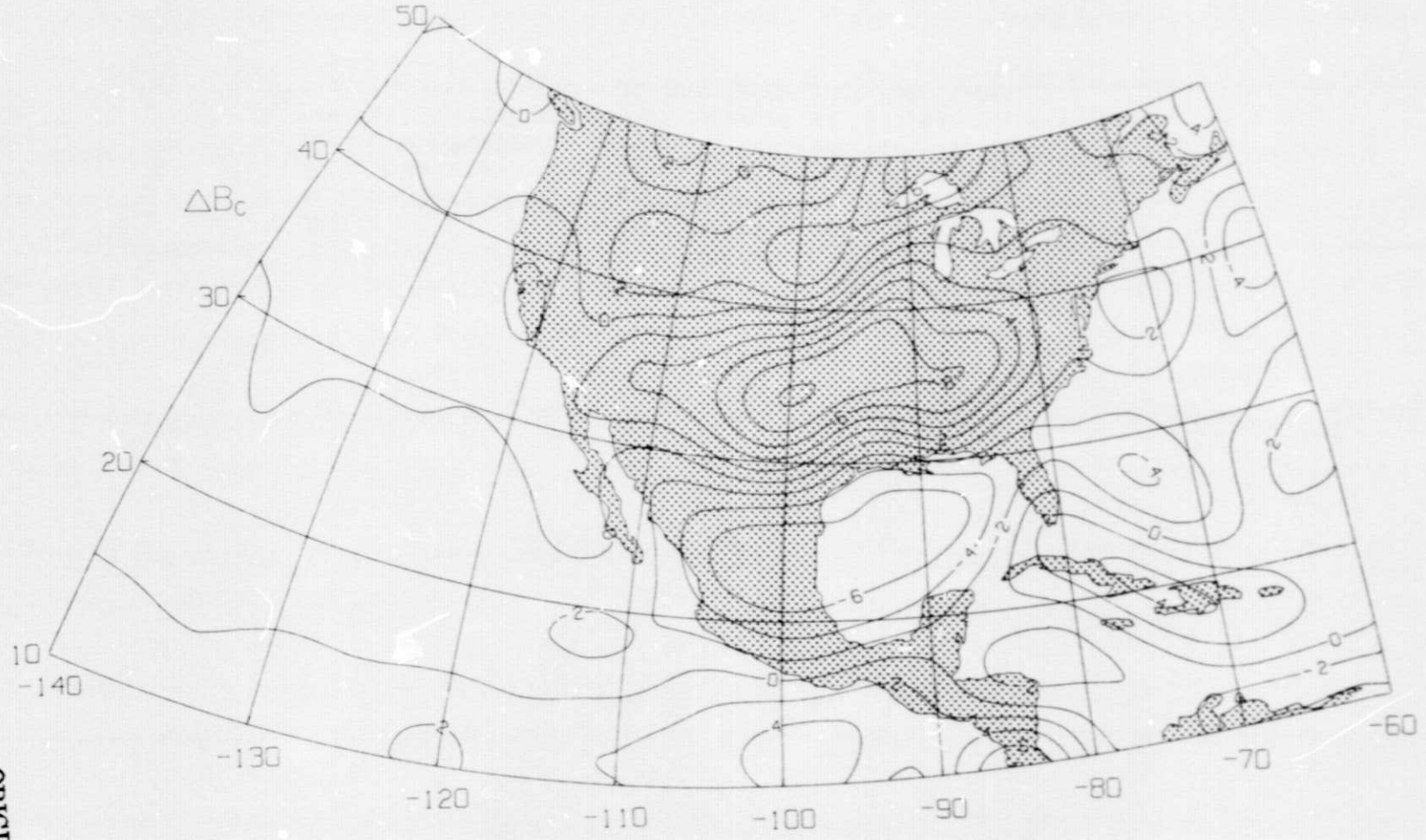

Figure 5: Anomaly field at 450 km computed from magnetization distribution of Figure 6. Units are nT.

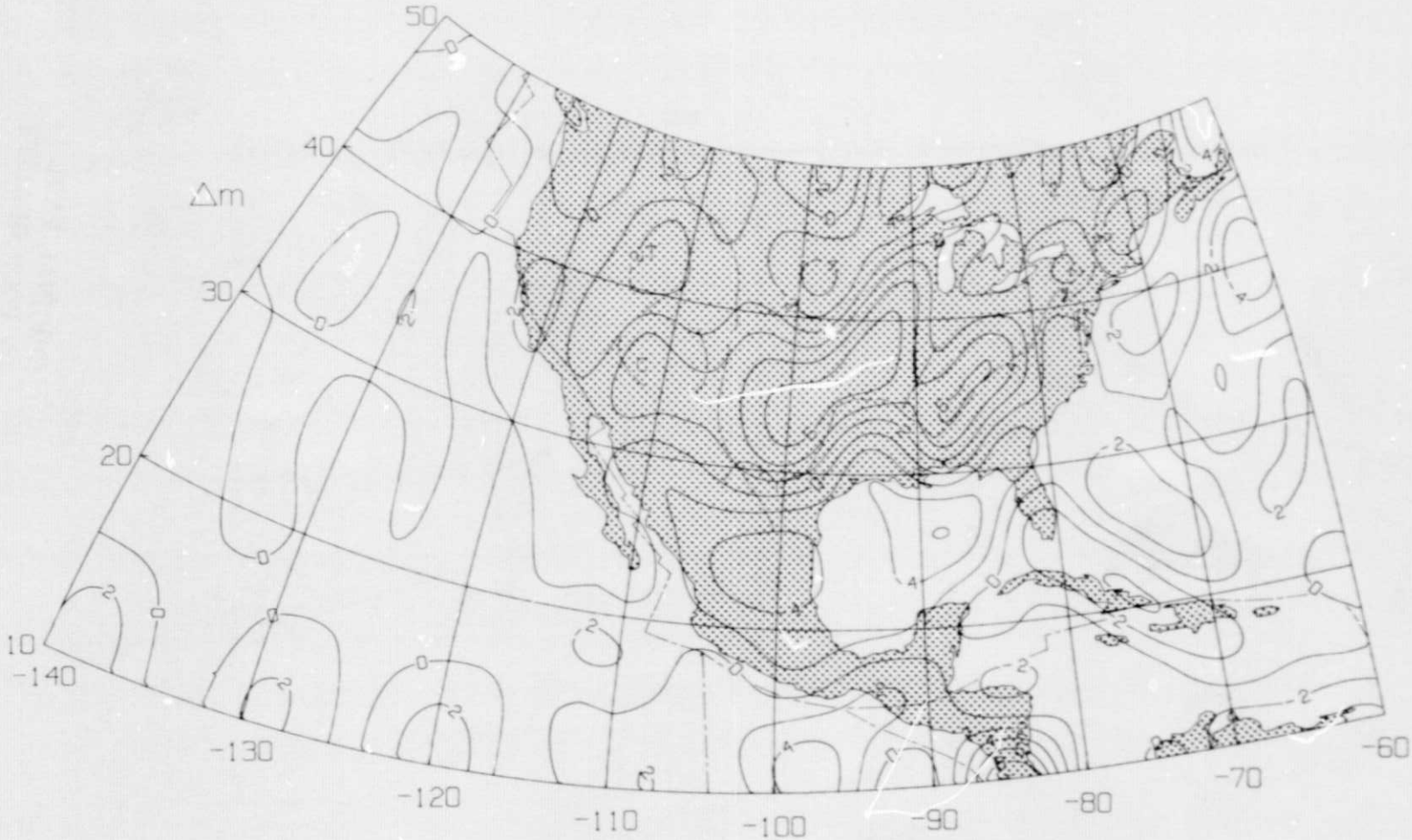

Figure 6: Magnetization distribution drom data of Figure 3. Units are emu/cc x 10^4. Tectonic boundaries shown are interior boundary of Appalachian-Ouachita system, eastern boundary of the Rocky Mountains, reactivated rift zone of Mississippi Embayment (Ervin and McGinnis, 1975), (C) Colorado Plateau, and (T) regional thermal anomaly of Eaton et al. (1976). Generalized plate boundaries shown as long dash-short dash lines.

Figure 7: 1^{o} average anomaly data (left) and magnetization distribution (right) from inversion of this data.

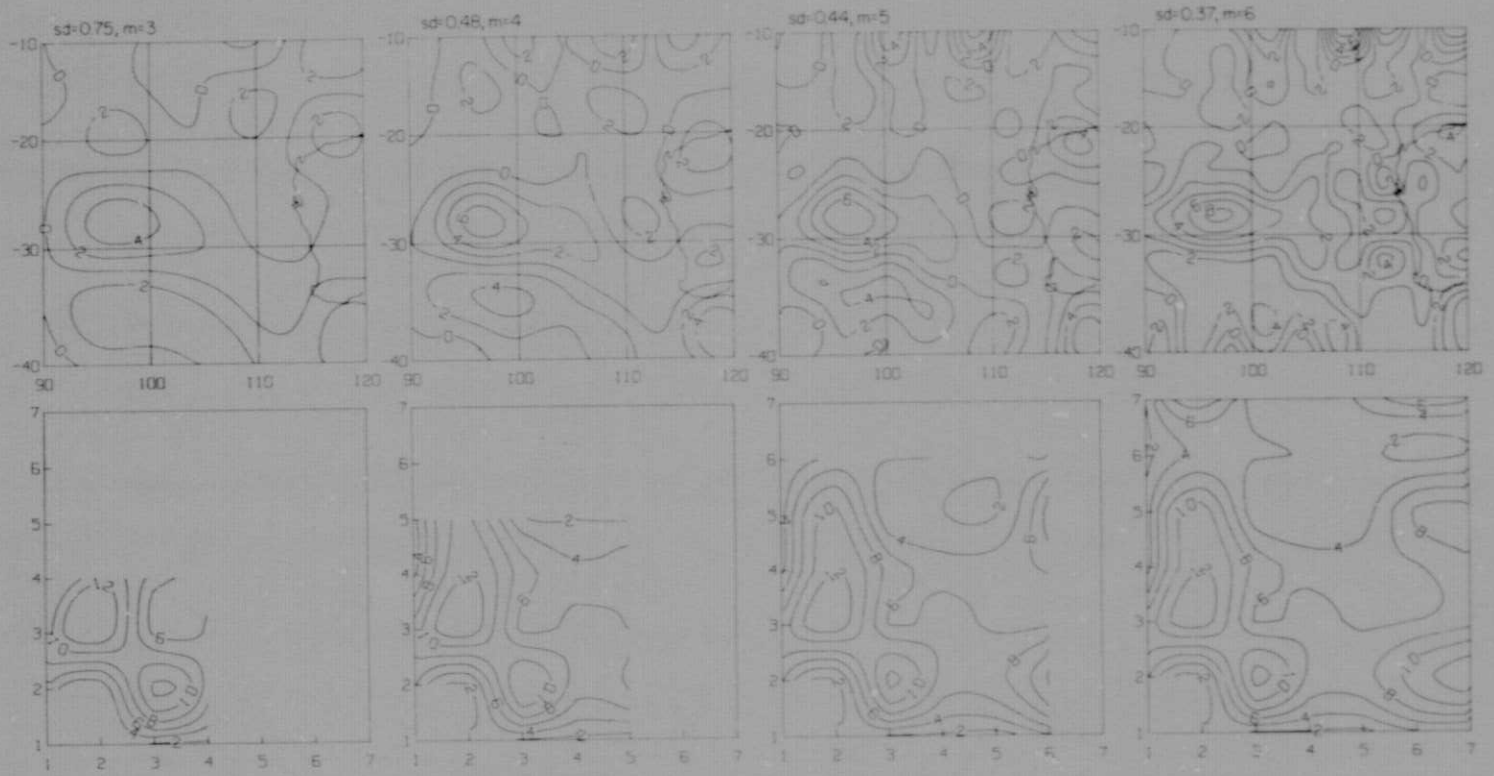

Figure 8: Magnetization distributions and corresponding power spectra for maximum wave number m= 3,4,5, and 6. Scale shown in wave number plus one.